Comparing two topology transformer hysteresis models derived from DC hysteresis measurements

Dennis Albert
Institute of Electrical Power Systems, Graz University of Technology, Graz, Austria

Lukas Daniel Domenig
Institute of Fundamentals and Theory of Electrical Engineering, Graz University of Technology, Graz, Austria

Philipp Schachinger
Institute of Electrical Power Systems, Graz University of Technology, Graz, Austria

Klaus Roppert
Institute of Fundamentals and Theory of Electrical Engineering, Graz University of Technology, Graz, Austria, and

Herwig Renner
Institute of Electrical Power Systems, Graz University of Technology, Graz, Austria

Received 5 September 2022
Revised 25 October 2022
19 December 2022
Accepted 23 January 2023

Abstract

Purpose – The purpose of this paper is to investigate the applicability of a direct current (DC) hysteresis measurement on power transformer terminals for the subsequent hysteresis model parametrization in transformer grey box topology models.

Design/methodology/approach – Two transformer topology models with two different hysteresis models are used together with a DC hysteresis measurement via the power transformer terminals to parameterize the hysteresis models by means of an optimization. The calculated current waveform with the derived model in the transformer no-load condition is compared to the measured no-load current waveforms to validate the model.

Findings – The proposed DC hysteresis measurement via the power transformer terminals is suitable to parametrize two hysteresis models implemented in transformer topology models to calculate the no-load current waveforms.

Originality/value – Different approaches for the measurement and utilization of transformer terminal measurements for the hysteresis model parametrization are discussed in literature. The transformer topology

COMPEL - The international journal for computation and mathematics in electrical and electronic engineering
Vol. 42 No. 4, 2023
pp. 861-877
Emerald Publishing Limited
0332-1649
DOI 10.1108/COMPEL-09-2022-0303

models, derived with the presented approach, are able to reproduce the transformer no-load current waveform with acceptable accuracy.

Keywords Magnetic hysteresis, Transient analysis, Transient simulation, Transformers

Paper type Research paper

1. Introduction

Transformer manufactures typically develop detailed models of the transformer based on the geometry and material properties to study the internal dielectric stresses, forces and heating. This detailed information is usually not available outside the manufacturer (da Co Rocha *et al.*, 2014). Therefore, transformer terminal equivalent models derived from terminal measurement, e.g. to study the transformer interaction with the surrounding grid, could be used (da Co Rocha *et al.*, 2014).

Different approaches are used to model transformers, according to the objective of the studies. Depending on the model structure and the procedure calculating the model parameters, the approaches can be classified as white or black box modelling. White box models require the knowledge of the structure of the transformer and the model parameters, which are derived with physical laws and do not depend on measurement data. The black box models, in contrast, depend on input and output parameters. The model structure and parameters have no physical meaning. Between the white and black box models, the grey box models offer a compromise between of both approaches. These topology models are usually based on the principle physical structure of the transformer, and the model parameter estimation is based on measurement data. In this paper, two transformer grey box models, using the inductance–reluctance (Cherry, 1949) and the capacitance–permeance analogy (Buntenbach, 1968, 1969), are used.

Both models are parameterized using the data from the standard factory acceptance test, including the transformer core hysteresis. The hysteresis characteristic is included because the deviation between the calculated and measured power demand should be within 15%, according to IEC 60076-1:2012. From the measured waveforms during factory acceptance test, the short-circuit impedance, the winding resistances, the winding capacitances, the three-phase no-load loss and the zero-sequence impedance can be calculated. The measurement procedures are described in IEC 60076-1:2012 (IEC, 2012). The model parameters are listed in Table A2. The transformer joint air gaps are modelled as non-linear saturation characteristic. The non-linear characteristic is derived from the direct current (DC) hysteresis measurement, whereas the data points above the knee point are derived with linear extrapolation. The non-linear air gap is based on the assumption that as the step-lap transformer core approaches saturation, the flux is forced also to neighbouring transformer sheets, increasing the flux path through air (see Figure A1). Further information on the air gap modelling can be found in Zirka *et al.*(2022) and Albert (2022). For further application also the residual flux inside the transformer core could be of interest, which requires to include a hysteresis model (Martinez and Mork, 2005). Especially, the modelling of the transformer core hysteresis properties, based on terminal measurements, is challenging, due to the magnetic coupling of the phases in multi-winding multi-leg power transformers (Albert, 2022). Different special transformer terminal measurement setups have been discussed to measure the transformer hysteresis characteristic in Neves and Dommel (1995), Fuchs and You(2002) and Albert *et al.* (2021). To mitigate the magnetic coupling in a three-phase three-leg two-winding power transformer, the alternating current (AC) saturation test was proposed in Albert *et al.* (2021). During the AC saturation test, depicted in Figure 5, the transformer in no-load condition is excited by two single-phase voltages via the outer two

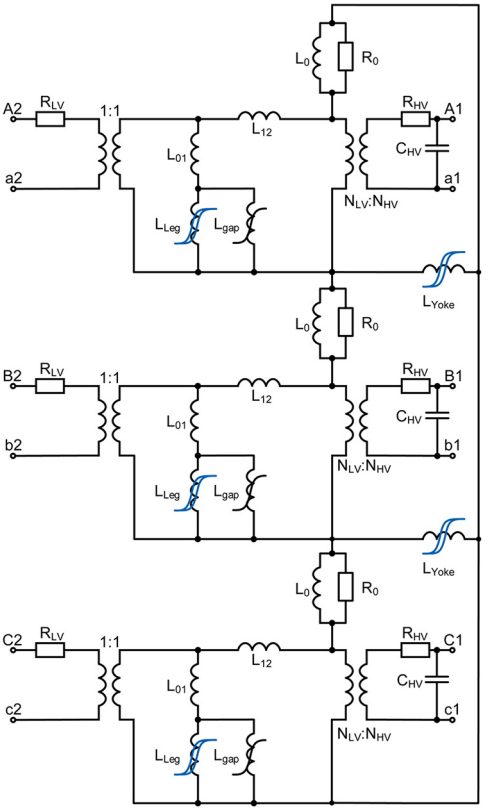

Figure 1.
Three-phase three-leg two-winding transformer model derived with inductance–reluctance analogy

wounded legs. The flux in the middle leg vanishes because of the 180° phase shift of the test voltages. The current waveforms were used in the subsequent modelling for the parametrization of the Jiles–Atherton (JA), used with the inductance–reluctance analogy, and capacitance–permeance hysteresis (CPH) model, used with the capacitance–permeance analogy, by means of an optimization with the Nelder–Mead Simplex (NMS) algorithm. The drawback of the AC saturation test is the requirement of a two-phase variable power source with a phase shift of 180°, sufficiently large power and a supply voltage which is above the rated voltage of the excited transformer windings. During the AC saturation, moderate saturation conditions can be reached, which requires a sufficiently large short-circuit power of the feeder. Therefore, the AC saturation test was further developed to a DC hysteresis test (depicted in Figure 5), which can be carried out with a portal transformer test device, at the manufacturers facility or on-site. During the DC hysteresis test, the same setup as with the AC saturation test is used. A DC step-voltage is applied to the transformer terminals several times with reversal polarity. The Ψ–i characteristic, derived from the terminal current and voltage measurements, is used for the subsequent hysteresis model parametrization. The hysteresis models are parametrized by simulating the DC hysteresis test with the transformer topological models in MATLAB/Simulink and applying a minimal cost function to the measured and calculated current waveforms during the optimization process.

2. Inductance–reluctance analogy

Using the inductance–reluctance analogy, based on Cherry (1949), the magnetic circuit of the transformer and its stray flux paths are represented by inductances in an electric equivalent circuit. This allows to model the magnetic and surrounding electric circuit in the electrical domain. The equivalent circuit of the transformer, applying the inductance–reluctance analogy, requires *first* that each element in one network has a counterpart in the other network and *second* the current through an element in one network is proportional to the voltage across the counterpart in the other network. These requirements are fulfilled by using the analogies listed in Table 1.

The inductance–reluctance analogy is limited to planar networks. A counter example where the analogy cannot be applied is given in Hamill (1993). This limitation can be overcome, if required, by the usage of five special artifices summarized in Bloch (1946).

Applying the inductance–reluctance analogy to the three-phase three-leg two-winding transformer under test, results in the equivalent circuit are depicted in Figure 1, where the upper-case letters A, B and C correspond to the high-voltage terminals/phases and the lower-case letters a, b and c correspond to the low-voltage terminals/phases. A and C represent the outer two legs and B the middle leg.

In Figure 1, L_{01} and L_{12} represent the leakage flux paths between the transformer core (index 0) and the inner winding (index 1), as well as the leakage flux path between the inner (index 1) and outer (index 2) winding, respectively. The elements R_0 and L_0 represent the zero-sequence flux path for each leg. R_{LV} and R_{HV} represent the low- and high-voltage winding resistance per phase, respectively. N_{LV} and N_{HV} are the number of turns of the corresponding winding. The inductor L_{gap} represents the air gap between the yoke and leg. It was found in Elleuch and Poloujadoff (1998) that the equivalent air gap length varies with the flux density. The effect of a changing equivalent air gap length can be represented by a non-linear inductor (Elleuch and Poloujadoff, 1998; Zirka *et al.*, 2022). The non-linear characteristic can be derived from DC hysteresis measurement by calculating a saturation characteristic from the hysteresis loop and linear extrapolating the saturation characteristic beyond the knee point. L_{yoke} and L_{leg} with the blue hysteresis symbol represent the corresponding hysteretical core elements of the legs and yokes. The inverse JA model, in the inductance–reluctance model (Jiles *et al.*, 1992; Jiles and Atherton, 1986), is used for the implementation of the transformer cores hysteresis characteristic, because it requires less measurement data than the Preisach hysteresis model (Philips *et al.*, 1995). Both the transformer legs and yokes are implemented as JA hysteresis model, using the same five JA model parameters. The hysteresis model takes into account the hysteresis losses, the rate

Table 1.
Analogies between electric and magnetic circuits

Magnetic circuit			Electric circuit		
mmf	$\mathcal{F} = \int H \mathrm{d}l$	A	Voltage	$V = \int E \mathrm{d}l$	V
Flux rate	$\dot{\Phi}$	V	Current	i	A
Reluctance	$\mathcal{R}$	H^{-1}	Inductance	L	H
Permeance	$\mathcal{P} = 1/\mathcal{R}$	H	Capacitance	C	F
Flux	$\Phi = \int \dot{\Phi} \mathrm{d}t$	Wb	Charge	$q = \int i \mathrm{d}t$	C
Permeability	$\mu = \mu_0 \mu_\mathrm{r}$	H/m	Permittivity	$e = e_0 e_\mathrm{r}$	F/m
Power	$P = F\dot{\Phi}$	W	Power	$P = vi$	W
Energy	$E = \int F \mathrm{d}\Phi$	J	Energy	$E = \int v \mathrm{d}q$	J

dependent excess losses and the eddy current losses. The total eddy current loses are derived from the three-phase no-load test and are multiplied by the total mean magnetic path length of the transformer core. The eddy current losses in every hysterical core element (L_{leg} and $L_{yoke)}$ are scaled with their specific length l_e. Figure 2 depicts one JA hysteresis element implemented in MATLAB/Simulink, where A is the core element's cross-sectional area; N_{LV} is the number of turns of the low-voltage winding; and $k20$ is the scaling factor for the rate-dependent excess loss. The dimensionless scaling factor $k20$ is roughly adjusted manually before the JA parameter optimization.

3. Capacitance–permeance analogy

The capacitance–permeance analogy or gyrator–capacitor approach is based on Buntenbach (1968, 1969). The analogies between the magnetic and electric circuit are listed in Table 2.

Applying the capacitance–permeance analogy to a transformer, the permeances of the magnetic circuit are translated into capacitances, representing the legs, yokes and the stray flux paths. The magnetic equivalent circuit is interfaced with a gyrator, connecting the surrounding electric circuit with the magnetic circuit. The gyrator is governed by the following relations:

$$I_1 = GV_2\,, \tag{1}$$

$$I_2 = GV_1\,, \tag{2}$$

where V_2 and I_2 correspond to the mmf $\mathcal{F}$ and the magnetic flux rate $\dot{\phi}$, respectively, and V_1 and I_1 correspond to the voltage and current of the external electrical circuit, respectively.

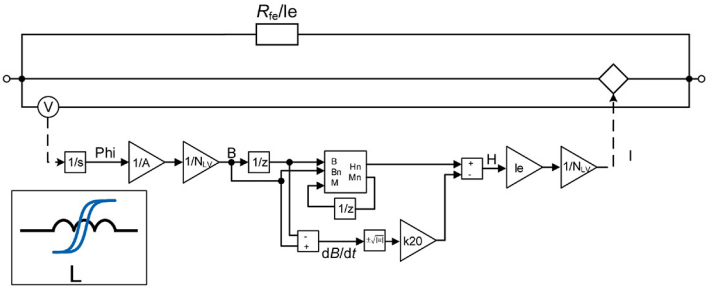

Figure 2.
Lumped circuit element for transformer leg and yoke with JA element

Magnetic circuit			Electric circuit		
mmf	$\mathcal{F}$	A	Voltage/emf	v	V
Flux rate	$\dot{\Phi}$	V	Current	i	A
Reluctance	$\mathcal{R}$	1/H	Resistance	R	Ω
Permeance	$\mathcal{P} = 1/\mathcal{R}$	H	Capacitance	C	F
Flux	$\Phi = \int \dot{\Phi} \mathrm{d}t$	Wb	Charge	$q = \int i \mathrm{d}t$	C
Power	$P = F\dot{\Phi}$	W	Power	$P = vi$	W

Table 2.
Capacitance–permeance analogy between electric and magnetic circuits

The resistance of the gyrator G is the reciprocal of N, the number of turns of the corresponding winding.

The capacitance – permeance analogy makes a capacitance on the electric domain analogous to a permeance in the magnetic domain. The two domains are linked as follows:

$$\dot{\phi} = \mathcal{P}\frac{\mathrm{d}\mathcal{F}}{\mathrm{d}t} \rightarrow \phi = \mathcal{P}\mathcal{F}. \tag{3}$$

Permeances are the reciprocal of reluctances and are defined as:

$$\mathcal{P} = \frac{1}{\mathcal{R}} = \frac{\mu_0 \mu_r A_e}{l_e}, \tag{4}$$

where l_e is the effective magnetic path length, A_e is the effective cross-sectional area, μ_0 is the vacuum permeability and μ_r is the relative permeability of the material. An electric resistance is used to model dissipating losses in the CPH model. This can be interpreted as a hampering of the magnetic flux rate. The resulting power loss is calculated as follows:

$$P_{\mathrm{loss}} = \dot{\phi}^2 R_{\mathrm{m}}. \tag{5}$$

The hysteretical lumped core elements (Figure 3) consist out of three building blocks. The saturation is modelled by a capacitor with a series connected non-linear voltage-controlled voltage source, with the following voltage–voltage relation:

$$E(V_{\mathrm{c}}) = (aV_{\mathrm{c}})^n, \tag{6}$$

where a and n are shape parameters. This results in an effective capacitance of:

$$C_{\mathrm{eff}} = \frac{C_s}{1 + \frac{\mathrm{dE}}{\mathrm{d}V_{\mathrm{c}}}}. \tag{7}$$

To model the hysteresis, a resistor and a parallel non-linear voltage-controlled current source are used. The voltage–current relation is defined as:

$$I(V_{\mathrm{h}}) = (bV_{\mathrm{h}})^m, \tag{8}$$

where b and m are shape parameters. The resistance for the hysteresis is non-linear to model a rate-independent hysteresis loop and to set the major loop to a certain limit. If a specific

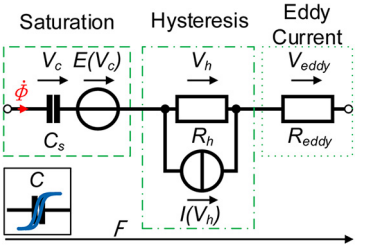

Figure 3.
Lumped circuit element for transformer leg and yoke with hysteresis, saturation and eddy current representation

value of V_c has been reached, most of the current in the hysteresis element flows through the current source, which limits the amount of current flowing in the resistance, which limits the dissipated power by the resistance and therefore the width of the hysteresis loop. To preserve the properties of (8) and (6) and to realize the saturation and the hysteresis (shape), the values of n and m have to be odd integers. For rate-dependent dissipative losses like eddy currents, a linear resistance can be used in series to the other elements. The material model is controlled by six parameters a, c, m, n, C_s and R_h.

The transformer model parameters are derived from the transformer factory acceptance test measurements. These measured parameters can be used directly in the inductance–reluctance analogy. For the usage in the capacitance–permeance analogy, the following conversions are applied to the measured parameters:

$$C = \frac{L}{N^2}\,, \tag{9}$$

where L is, e.g. the leakage inductance and N are the number of turns of the inductor representing the leakage flux path, which is chosen to be $N = 1$, since the leakage flux paths correspond to an air coil with one turn. The equivalent circuit of a three-phase three-leg two-winding transformer, applying the capacitance–permeance analogy, is depicted in Figure 4.

In Figure 4, 1X-1x represents the high-voltage terminals and 2X-2x represents the low-voltage terminals of the corresponding phase (X/x = A/a, B/b, C/c). The hysteretical leg and yoke elements (C_{leg} and C_{yoke}) are indicated by the blue hysteresis loop above the capacitor. The flux-shunting elements C_{01}, C_{12} and C_0 represent the leakage flux paths between the core and the inner winding (index 1), the leakage flux path between the inner and outer (index 2) winding and the zero-sequence flux path (index 0), respectively.

4. DC hysteresis measurement

For the accurate modelling of transformers for low-frequency transients, the model should include the transformer core hysteresis effect (Martinez and Mork, 2005). If the core material and its hysteresis characteristic is unknown, transformer terminal measurements and the corresponding Ψ–i or Φ–i characteristic can be used to parameterize the transformer hysteresis model. The derived Ψ–i characteristics from a three-phase no-load test have limited value, due to the electromagnetic coupling of the three phases (Albert, 2022; Fuchs and You, 2002). Therefore, different single-phase measurement techniques have been proposed in Fuchs and You (2002) and Albert *et al.* (2021). Both measurement techniques are performed at the transformers' rated frequency, usually 50 or 60 Hz. The testing with rated frequency requires a sufficiently large power source for the tests, which limits the

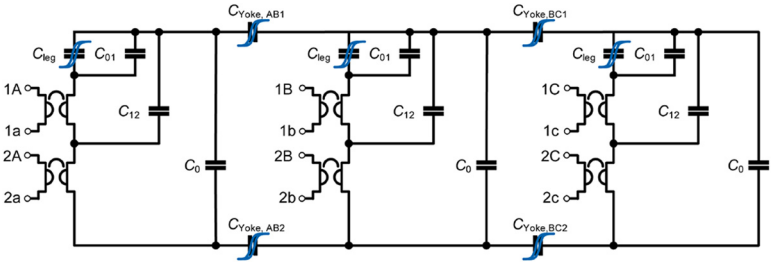

Figure 4.
Three-phase three-leg two-winding transformer model derived with capacitance – permeance analogy

measurement techniques to transformers in test facilities or to transformers with small rated power. To overcome this limitation, a similar test, as proposed in Albert *et al.* (2021), with DC is used to measure the data for the subsequent hysteresis modelling, with a portable transformer test device. Figure 5 depicts the AC saturation test, proposed in Albert *et al.* (2021) and the DC hysteresis test. In Figure 5, only one winding per leg is depicted for a better visualization, whereas the AC saturation test is usually carried out via the low-voltage terminals and the DC hysteresis test is carried out via the high-voltage terminals. With both measurement techniques, the flux in the middle leg vanishes, which reduces the electromagnetic coupling.

Plate 1 depicts the transformer under test in the laboratory. The high-voltage neutral was made accessible from outside via a high-voltage bushing. The six low-voltage windings from the zigzag winding were feed through the transformer tank with a connector box. The low-voltage winding vector group is free configurable from outside. For the presented measurement, the transformer was in YNyn0 connection. The transformer core dimensions and the characteristic data of the transformer are listed in Table A1 and Table A2, respectively.

Figure 6 depicts a typical measured voltage and current waveform of the transformer under test with the labelled sequences explained in Table 3.

Figure 7 presents the measured transformer under test $\Phi - i$ hysteresis characteristic derived from transformer terminal measurements. The AC and DC hysteresis characteristic are derived from the AC saturation and DC hysteresis test via the low-voltage and high-voltage terminals A-C, respectively. The "ringing", visible in the DC hysteresis measurement around 0 A, is caused by control parameters in the transformer test device at low current. Clearly visible is the smaller width of the DC hysteresis measurement, due to the absence of rate-dependent and eddy current losses. The "cobra-shape" of the AC hysteresis characteristic is an indicator for the effect of the winding capacitance and the transformer core joint air gap.

During the optimization of the hysteresis parameters of the CPH and JA models, the measured and calculated currents during the DC hysteresis test are used, using the NMS algorithm implemented in MATLAB as function fminsearch() (Lagarias *et al.*, 1998). During the optimization, the objective function is defined as the sum of the squared error between the calculated and measured phase currents of the DC hysteresis test, where also the maximum and minimum currents values during the interval used for the optimization are compared. The objective function is defined as follows:

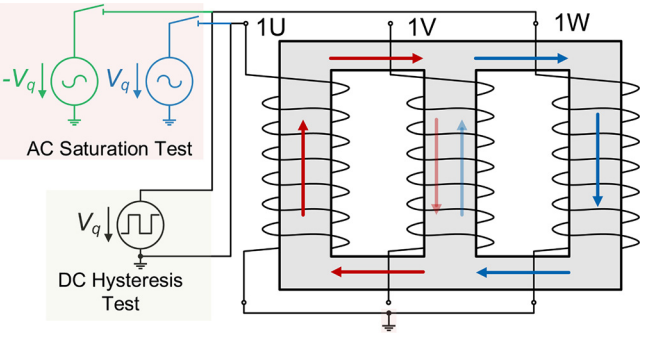

Figure 5.
AC saturation and DC hysteresis test setup on a three-phase two-winding transformer

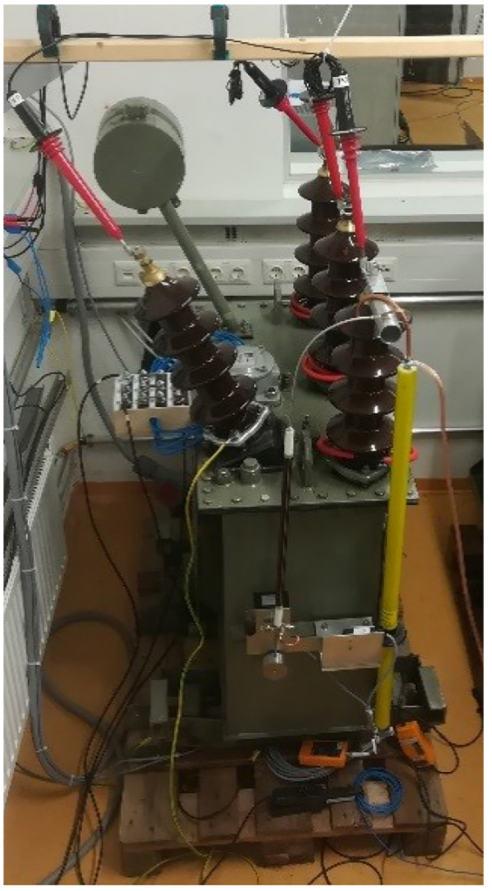

Plate 1.
50 kVA modified transformer under test in the laboratory

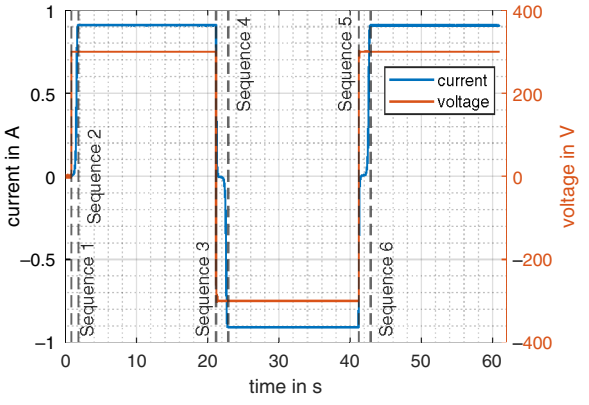

Figure 6.
Measured voltage and current waveform during DC hysteresis test on the transformer under test via the high-voltage terminals A-C

$$J = k_1 J_1 + k_2 J_2 = \frac{1}{M}\sum_{i=1}^{M} k_1 \left[I_{\mathrm{calc}}(i) - I_{\mathrm{meas}}(i)\right]^2 + k_2 \left[I_{\mathrm{max,sim}} - I_{\mathrm{max,calc}}\right]^2, \quad (10)$$

where I are the measured (meas) and calculated (calc) phase currents; k_1 and k_2 are weighting parameters, which are chosen by trial-and-error method; and M are the number of data points. The results of the models, using the hysteresis parameters from the optimization, are depicted in Figures 8 and 10 in the following sections. Other parameters used in the objective function, such as the frequency spectrum of the current waveforms or the B–H or Φ–i values, did not result in suitable hysteresis parameters. Therefore, current waveform versus time and its maxima and minima should be used in the objective function.

5. Model validation: inductance–reluctance model

The parameters of the hysteresis models (JA and CPH) used in the lumped elements for the legs and yokes are parameterized by means of an optimization, using the NMS algorithm, where the measured and calculated terminal currents of the transformer during the DC hysteresis test are compared. Figure 8 depicts the measured and calculated current and voltage waveform after the optimization process of the JA hysteresis parameters. The total DC hysteresis measurement sequence, depicted in Figure 6 with a duration of 62 s, was reduced to a sequence with a duration of 4.5 s to limit the simulation time per iteration during the optimization. This is applicable, due to the symmetry of the hysteresis characteristic. The depicted excerpt in Figure 8 takes into account the initial magnetization and the descending branch from the positive maximum magnetization to negative

Table 3. Sequences during DC hysteresis test, according to Figure 6

Sequence	Voltage	Current	Hysteresis characteristic part
1	+DC	$\Delta I > 0$	Positive saturation; anhysteretic curve
2	Steady-state conditions		
3	−DC	$\Delta I < 0$	Negative saturation, descending hysteresis branch
4	Steady-state conditions		
5	+DC	$\Delta I > 0$	Positive saturation, ascending hysteresis branch
6	Steady-state conditions		

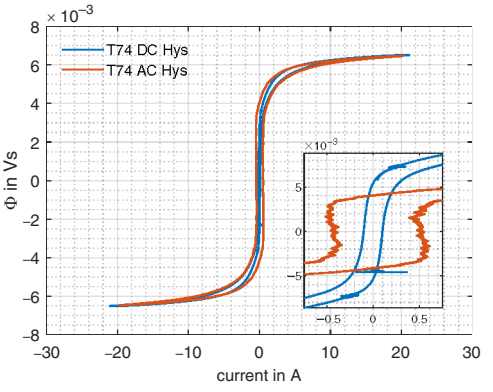

Figure 7. Comparison of the Φ–i DC and AC hysteresis characteristic of the transformer under test, measured via the low-voltage terminals A-C

maximum magnetization point. The voltage "ringing" at 2.2 s is caused by the control parameters of the portable transformer test device.

The derived JA hysteresis model parameters obtained from the optimization are used in the same transformer model during the standard no-load test to validate the model. The model parameters are listed in Table 5. Figure 9 depicts the measured and calculated three-phase no-load voltage and current waveforms of the transformer under test. The current amplitude and waveform shape are similar. The calculated power in the model underestimates the measured power but have the same order of magnitude (Table 4).

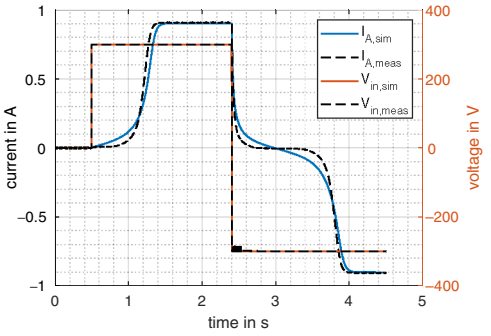

Figure 8. Calculated and measured DC hysteresis test with identified JA hysteresis parameters

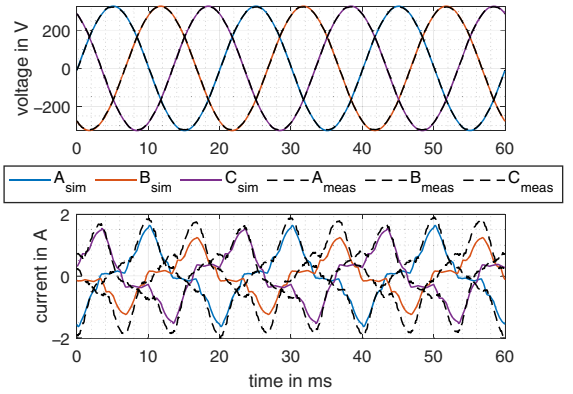

Figure 9. Comparison of calculated and measured current waveforms, derived from the DC hysteresis test of the transformer under test

Table 4. Power demand comparison for no-load test with model parameters derived from the DC hysteresis test with inductance–reluctance model

Power	Calculated	Measured	Deviation	Deviation in (%)
S in VA	497.4	650.9	153.5	23.6
Q_t in var	467.0	629.7	164.7	25.8
Q_1 in var	459.3	585.8	126.5	21.6
P in W	171.3	164.6	6.7	4.1

Further improvements of the optimization process and especially of the applied minimal cost function should decrease the deviation in the power demand (Table 5).

6. Model validation: capacitance–permeance model

The results of the optimization process are shown in Figure 10. It can be seen that the capacitance–permeance model is able to reproduce the measured current waveform by applying the DC hysteresis test with a high accuracy. However, compared to the AC saturation test, this is only possible using the topology of the lumped elements, as shown in Figure 4. This means each leg and yoke has to be modelled as an individual element to take into account the transformer core geometry and the stray flux paths. The transformers joint air gap is modelled as a linear capacitance in series to the hysteresis element.

The same model as in the DC hysteresis test is subsequently used for the no-load test to validate the identified hysteresis parameter and the overall model. The CPH model parameters are listed in Table 7. In Figure 11, the measured and simulated time evolution of the current and voltage in all phases is compared. It can be recognized that also during the no-load test, the model is able to predict the terminal currents and the power demand (Table 6) with an acceptable accuracy. The minor deviations are most likely due to several inhomogeneities which cannot be modelled with the current version of the topology model like an inhomogeneous distribution of the magnetic flux density in the core, as well as different air gaps in the leg and yoke and different leakage levels of the windings, which has not been considered in the model yet (Table 7).

7. Conclusion

This paper presents the feasibility of using a transformer terminal DC hysteresis measurement to parameterize two different hysteresis models in transformer grey box topology models. The derived models are able to reproduce the measured current

Table 5.
Hysteresis model parameters derived with the DC hysteresis test

Jiles–Atherton hysteresis parameters				
M_s	α	k	a	c
$3.217 \cdot 10^6$	$171.9 \cdot 10^{-6}$	14.12	209.54	0.2004

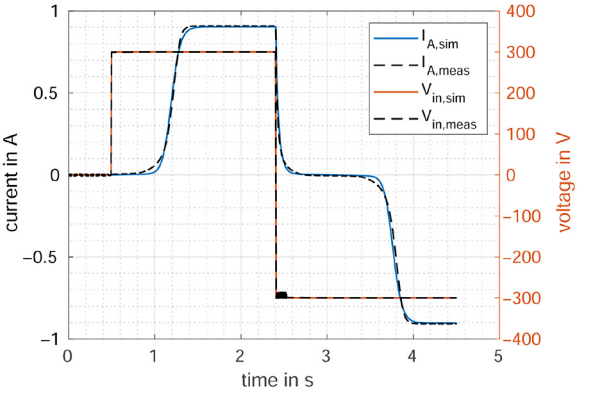

Figure 10.
Calculated and measured DC hysteresis test with identified CPH parameters

waveforms and power demand during the standard no-load test. The parameters of the inductance–reluctance model can be recalculated for the usage in the capacitance–permeance model and vice versa. The capacitance–permeance model is more intuitive because the core design with its legs and yokes do not need to be transformed, as it is the case if the inductance–reluctance analogy is used, to set up the equivalent electric transformer topology model. The five and six parameters of the JA and the CPH models, respectively, are derived by means of an optimization with the NMS algorithm and an objective function. An excerpt of the measured and calculated current waveform during the DC hysteresis test was used during the optimization to reduce the simulation time per iteration. The approach was tested on a 50 kVA three-phase three-leg two-winding transformer. For the topology model, the factory acceptance test data is required to parameterize the model parameters, such as the leakage inductances, zero-sequence impedance, winding resistance, winding capacitance and iron core losses. Furthermore, the core geometry of the transformer is required, which is not always available. The

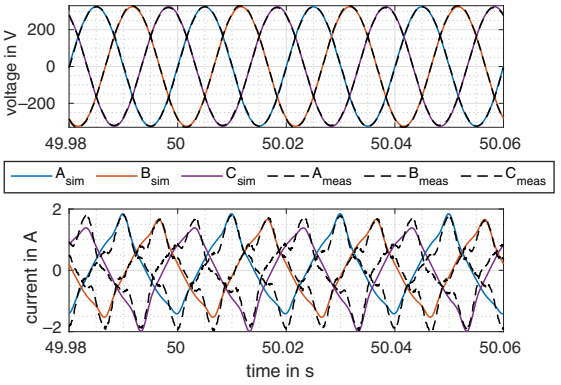

Figure 11.
No-load test with identified CPH parameter derived from the DC test

Table 6.
Power demand comparison for no-load test with model parameters derived from the DC hysteresis test with capacitance–permeance model

Power	Calculated	Measured	Deviation	Deviation in %
S in VA	665.6	650.9	14.65	2.25
Q_t in var	641.2	629.7	11.5	1.82
Q_l in var	641.2	585.8	55.4	9.45
P in W	178.4	164.6	13.8	8.3

Table 7.
Hysteresis model parameters derived with the DC hysteresis test

CPH parameters					
C_s	R_h	a	b	n	m
0.0107	6.9297	1.4953	0.0548	13.0	31.0

derived models are able to reproduce the measured no-load current waveform and power no-load power demand with acceptable accuracy. The calculated power demand of the inductance–reluctance model with the JA hysteresis model is sensitive to the calculation step size.

The discrepancy between the two models presented in Sections 2 and 3 in the current waveform and in power demand is expected to be caused by the air gap inductance in combination with the CPH model parameters and the step size in combination with the power calculation method in the inductance–reluctance model. The current waveform of the capacitance–permeance model is more linear between the current peaks, in comparison with the inductance–reluctance model, even if the same air gap values are used in the models. By reducing the air gap capacitance in the CPH model before the optimization, the current waveforms during the three-phase no-load test become similar to the measured phase currents. The discrepancy in the power demand between both models is expected to be caused by the power calculation in MATLAB/Simulink in combination with the simulation step size, especially in case of the inductance–reluctance model. If the step size is reduced in the calculation of the inductance–reluctance model, the power demand deviation can also be reduced. The effect of the calculation step size can also be observed by comparing the $\Phi - i$ characteristics during the DC hysteresis test of both models with different step sizes. The inductance–hysteresis model with the JA hysteresis model shows dedicated steps in the $\Phi - i$ characteristic, if the step size is chosen too large. This behaviour also affects the power calculation in the model.

The paper presents two transformer topology models, including the transformer core hysteresis. Both models are able to reproduce the three-phase current waveform and the power demand with a certain accuracy. Which analogy and hysteresis model should be used depends on the application and will be investigated in future work. The inductance–reluctance model requires sufficiently small calculation step sizes to provide smooth current waveforms, which requires a higher computational power in comparison to the capacitance–permeance model. Today, the inductance–reluctance analogy is more common in electrical power engineering, whereas the capacitance–permeance analogy is more used in the field of electronic circuit simulation. Both models can be parameterized using the same data.

The presented approach using a DC hysteresis measurement has the advantage that it can be conducted on-site on at the manufactures site or on an already installed transformer. This allows to build an electromagnetic model of a transformer, based on measurements which can be conducted with a portable transformer test device. Thus, an electromagnetic model of a transformer can be derived, even if detailed or specific information is no longer or not available. The approach can be used in future, e.g. to determine the increased power demand of step-up transformers in power generation units, where power electronic converters are replacing an existing motor-generator. The retrofitting of power electronic converters in power generating units usually requires a new assessment of the losses caused by higher frequency components in the generation unit. Further work will focus on the model validation under different operation conditions to define the scope of applicability of the model. It will include inrush current calculation, short-circuit test, zero-sequence test and back-to-back operation with and without superimposed DC. Regarding the power demand, of special interest is the accuracy of the derived model, when exposing the transformer to distorted voltage waveform, such as the ones caused by power electronic converters.

References

Albert, D. (2022), "Analysis of power transformers under DC/GIC bias", PhD Thesis, Graz University of Technology, Graz, Austria.

Albert, D., Domenig, L., Maletic, D., Reinbacher-Köstinger, A., Roppert, K. and Renner, H. (2022). "Comparing two topology transformer hysteresis models with power transformer measurements", *2022 23rd International Conference on the Computation of Electromagnetic Fields (COMPUMAG)*, IEEE, pp. 1-4.

Albert, D., Maletic, D. and Renner, H. (2021), "Measurement based transformer modelling approach", In ETG Congress 2021, VDE, pp. 1-6.

Bloch, A. (1946), "On methods for the construction of networks dual to non-planar networks", *Proceedings of the Physical Society*, Vol. 58 No. 6, p. 677.

Buntenbach, R. (1968), "Improved circuit models for inductors wound on dissipative magnetic cores (circuit models for inductors wound on dissipative magnetic cores)".

Buntenbach, R.W. (1969), "Analogs between magnetic and electrical circuits", *Electronic Products Magazine*, Vol. 12 No. 5, p. 108.

Cherry, E.C. (1949), "The duality between interlinked electric and magnetic circuits and the formation of transformer equivalent circuits", *Proceedings of the Physical Society. Section B*, Vol. 62 No. 2, p. 101.

da Co Rocha, A., Holdyk, A., Gustavsen, B., Jaarsveld, B.J., Portillo, A. and Popov, M. (2014), "Electrical transient interaction between transformers and the power system-Part 2", Case studies.

Elleuch, M. and Poloujadoff, M. (1998), "New transformer model including joint air gaps and lamination anisotropy", *IEEE Transactions on Magnetics*, Vol. 34 No. 5, pp. 3701-3711.

Fuchs, E.F. and You, Y. (2002), "Measurement of Psi-i characteristics of asymmetric three-phase transformers and their applications", *IEEE Power Engineering Review*, Vol. 22 No. 8, pp. 69-70.

Hamill, D.C. (1993), "Lumped equivalent circuits of magnetic components: the gyrator-capacitor approach", *IEEE Transactions on Power Electronics*, Vol. 8 No. 2, pp. 97-103.

IEC (2012), "Power transformers part 1: General".

Jiles, D.C. and Atherton, D.L. (1986), "Theory of ferromagnetic hysteresis", *Journal of Magnetism and Magnetic Materials*, Vol. 61 Nos 1/2, pp. 48-60.

Jiles, D.C., Thoelke, J.B. and Devine, M.K. (1992), "Numerical determination of hysteresis parameters for the modeling of magnetic properties using the theory of ferromagnetic hysteresis", *IEEE Transactions on Magnetics*, Vol. 28 No. 1, pp. 27-35.

Lagarias, J.C., Reeds, J.A., Wright, M.H. and Wright, P.E. (1998), "Convergence properties of the Nelder–Mead simplex method in low dimensions", *SIAM Journal on Optimization*, Vol. 9 No. 1, pp. 112-147.

Martinez, J.A. and Mork, B.A. (2005), "Transformer modeling for low-and mid-frequency transients – a review", *IEEE Transactions on Power Delivery*, Vol. 20 No. 2, pp. 1625-1632.

Neves, W.L. and Dommel, H.W. (1995), "Saturation curves of delta-connected transformers from measurements", *IEEE Transactions on Power Delivery*, Vol. 10 No. 3, pp. 1432-1437.

Philips, D.A., Dupre, L.R. and Melkebeek, J.A. (1995), "Comparison of Jiles and Preisach hysteresis models in magnetodynamics", *IEEE Transactions on Magnetics*, Vol. 31 No. 6, pp. 3551-3553.

Zirka, S.E., Albert, D., Moroz, Y.I. and Renner, H. (2022), "Further improvements in topological transformer model covering core saturation", *IEEE Access*, Vol. 10, pp. 64018-64027.

Appendix

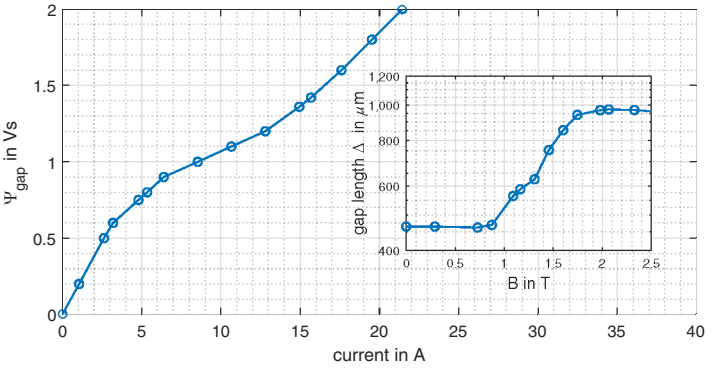

Figure A1.
$\Psi - i$ characteristic of non-linear air gap in inductance – reluctance and capacitance – permeance model and corresponding length change versus flux density B

Table A1.
Core dimensions of transformer under test

Core section	Cross-sectional area mm^2	Length mm
Leg	6740	330
Yoke	6740	230

Table A2.
Transformer under test parameters referred to low-voltage side

Voltages (phase-to-ground, rms) V_{LV}/V_{HV} in kV	16.0/0.23
Winding resistances R_{LV}/R_{HV} in Ω	321/0.034
No-load loss P_{fe} in W	163
Short-circuit reactance X_{12} in Ω	0.228
Short-circuit inductance L_{12} in mH	0.73
Zero-sequence inductance L_0 in mH	8.67
Zero-sequence resistance R_0 in Ω	3.75
Winding capacitance C_{HV} to ground in nF	3
Number of turns N_{HV}/N_{LV}	7730/102
Scaling factor k20	415

About the authors

Dennis Albert received the master's degree in electrical engineering from RWTH Aachen University, Germany, and the PhD in electrical engineering from Graz University of Technology in 2022. Since 2022, he is working as an application engineer at OMCIRON electronics GmbH in Austria. His field of research includes power transformer modelling and diagnostics. Dennis Albert is the corresponding author and can be contacted at: dennis.albert@tugraz.at

Lukas Daniel Domenig is a PhD student at the Institute of Fundamentals and Theory in Electrical Engineering at Graz University of Technology, Austria. His main research interests are electromagnetic network models and finite element methods including hysteresis operators.

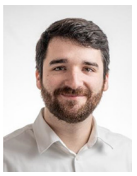

Philipp Schachinger received his master's degree in electrical engineering from Graz University of Technology in 2019. Since 2019, he is pursuing his PhD thesis at the Department of Electrical Power Systems at Graz University of Technology. His research focuses on the influence of solar storms on power grids and grid calculation.

Klaus Roppert received his master's degree in mechanical engineering in 2017 and his PhD in 2020 at Vienna University of Technology. Since 2020, he is a postdoc at the Institute of Fundamentals and Theory in Electrical Engineering and head of the multiphysical modelling and simulation group. His main research interests are computational multiphysics, magnetic material modelling and low-frequency approximations of electromagnetic field problems.

Herwig Renner received the PhD in 1995 and his habilitation in 2003 at Graz University of Technology, where he works as Associate Professor at the Department of Electrical Power Systems. His main research work is in the area of electrical power quality and power system dynamics. He is a member of CIRED technical committee and several CIGRE working groups.